Frontiers in Mechanochemistry and Mechanical Alloying

INCOME2008
1-4 December, 2008

MECHANOSORPTION OF CO_2 BY SILICATES: MECHANISM, KINETICS AND POSSIBLE APPLICATIONS

A.M. Kalinkin[ξ]
I.V. Tananaev Institute of Chemistry and Technology of Rare Elements and Mineral Raw Materials
Kola Science Center of RAS, Apatity, Russia

Keywords: Silicates, Carbon dioxide, Mechanosorption

Abstract

Mechanically induced CO_2 extensive sorption by silicate minerals (labradorite, diopside, okermanite, ghelenite, and wollastonite) has been considered. The silicates mechanically activated in CO_2 atmosphere in a planetary mill AGO-2 have been characterized using XRD and IR spectroscopy. Micro- and nanostructure of material resulting from mechanochemical interaction of diopside with CO_2 were investigated using SEM and TEM. The obtained data suggest that CO_2 penetrates the structurally disordered silicate matrix and "dissolves" in the particles volume with formation of homogeneous carbonate-silicate phase. Equations that reasonably good represent kinetics of CO_2 mechanosorption by the silicates have been proposed. These equations enable to calculate mechanosorption coefficients characterizing the diffusivity of CO_2 into disordered silicate matrix under intensive mechanical impact. Correlations between CO_2 content in mechanically activated silicates and CO_2 solubility in the corresponding melts, as well as between mechanosorption coefficients and CO_2 diffusion coefficients in the melts have been revealed. Possible application of the revealed effect in improving of alkali-activated ferrous-magnesium slag binding materials has been discussed.

Introduction

This work is a part of our systematic study of mechanochemical interaction between silicates, complex oxides and CO_2. It started from revealing of unusual reactivity increase of calcium and magnesium containing silicates such as diopside $CaMgSi_2O_6$, wollastonite $CaSiO_3$ and others with respect to carbon dioxide during fine grinding in a mortar in air or during mechanical activation (MA) in a planetary mill in CO_2 atmosphere [1,2]. The silicates, which are virtually inert to CO_2 at ambient conditions without mechanical impact, selectively consume carbon dioxide from the environment in the form of carbonate ions in amount comparable with Ca and Mg content in the minerals. In that case, one might expect occurring of reaction yielding corresponding carbonates and silica, e.g.:

$$\tfrac{1}{2}\, CaMgSi_2O_6(\text{diopside}) + CO_2 = \tfrac{1}{2}\, CaCO_3(\text{calcite}) + \tfrac{1}{2}\, MgCO_3(\text{magnesite}) + SiO_2$$

However, no reflections of carbonates or other crystalline phases were observed in XRD patterns of MA-silicates. It was shown that extensive mechanically induced carbonization of the silicates does not result in formation of amorphous carbonate and could not be explained by CO_2 chemisorption on the surface of the silicate particles. The obtained data suggest that CO_2 penetrates the structurally disordered silicate matrix and "dissolves" in the particles volume with formation of carbonate-silicate phase as a result of deep mechanosorption [1-4]. According to IR spectroscopic data this phase resembles finely ground glass obtained by quenching of silicate melt wherein CO_2 was dissolved at magma state conditions (T~1800-2000 K, P~1-2 GPa) [1,2]. Remarkable is the fact that the dissolution of carbon dioxide in the melts occurs only under conditions of high temperature and pressure, while in our experiments, silicates consume CO_2 during MA under ambient conditions. Similar to glass, product of mechanochemical interaction between alkaline earth silicates and CO_2 is thermodynamically unstable but kinetically stable substance. It does not change its chemical composition and amorphous state during storage in desiccator at least for several years.

As distinct from Ca and Mg silicates, mechanochemical interaction of Na and K silicates with CO_2 is an ordinary substitution reaction. The products of this reaction are amorphous silica and corresponding alkali metal carbonates or hydrogen carbonates as was substantiated by XRD data [5,6].This difference in interaction is caused by two main factors. First, for alkaline earth metal silicates, carbonization reaction like reaction (i) is thermodynamically less favorable than corresponding reactions for alkali metal silicates. Second, there are kinetic limitations related to melting temperatures of the silicates and their hygroscopic properties [5,6]. Practical application of the revealed effect deals with purposeful modification of particles outer layers in order to increase their reactivity, e.g. to improve binding or sorption properties. In principle, deep mechanosorption can be used for selective sorption of CO_2 from gas mixtures.

In this paper structural and chemical changes of natural and synthetic silicate minerals (labradorite, diopside, okermanite, ghelenite, and wollastonite) in the course of MA in CO_2 atmosphere have been studied. Transmission electron microscopy (TEM) data supporting hypothesis of mechanically induced "dissolution" of carbon dioxide in the structurally disordered silicate with formation of homogeneous amorphous carbonate–silicate phase have been obtained. Equations that reasonably good represent kinetics of CO_2 mechanosorption by the silicates have been proposed. Correlations between carbon dioxide mechanosorption by silicates and CO_2 dissolution in silicate melts have been revealed. CO_2 mechanosorption by magnesium-ferrous slag for improving of its binding properties has been considered.

[ξ] email : kalinkin@chemy.kolasc.net.ru

Table 1. Chemical composition of labradorite, diopside, okermanite, ghelenite, and wollastonite samples (wt. %)

Sample	SiO_2	Al_2O_3	CaO	Na_2O	K_2O	FeO	Fe_2O_3	MgO	TiO_2
Labradorite	53.7±0.5	26.3±0.2	10.80±0.10	4.65±0.05	0.45±0.03	1.62±0.05	0.61±0.05	1.03±0.05	0.28±0.02
Diopside	49.7±0.5	1.34±0.05	24.50±0.15	0.43±0.05	0.19±0.02	2.88±0.05	-	16.10±0.10	0.48±0.05
Okermanite	42.4±0.5	3.60±0.05	34.5±0.2	1.80±0.05	0.10±0.02	2.75±0.05	-	9.40±0.10	-
Ghelenite	21.92	37.18	40.90	-	-	-	-	-	-
Wollastonite	51.72	-	48.28	-	-	-	-	-	-

Experimental

Samples

Natural plagioclase, diopside, okermanite and synthetic ghelenite and wollastonite samples were used for experiments. Chemical composition of the minerals is given in Table 1. Plagioclase sample (fraction -250+125 μm) was from Gorodische deposit (Ukraine). It contained less than 1 mass % of magnetite as admixture. Plagioclases form discontinuous solid solutions from anorthite $CaAl_2Si_2O_8$ to albite $NaAlSi_3O_8$ by substitution of Ca and Al for Na and Si. According to CaO/Na_2O percentage (Table 1) the plagioclase sample can be classified as labradorite [7]. Both diopside and okermanite samples (fractions -200+125 μm) were from Kovdor deposit (Kola Peninsula, Russia) and contained less than 1% of carbonates and micas as admixtures.

Ghelenite $Ca_2Al_2SiO_7$ and wollastonite $CaSiO_3$ were synthesized from reagent grade $CaCO_3$, Al_2O_3 and amorphous silica. Before synthesis calcium carbonate was heated at 200°C for 24 h. Alumina and amorphous silica were annealed at 1000°C for 12 h. Stoichiometric mixtures of the components in both cases were ground in a Fritsch Pulverisette 2 laboratory mortar grinder for 10 h. After grinding mixtures were annealed at 900°C for 8 h and then at 1300°C for 12 h. Grinding for 10 h and annealing at 1300°C for 12 h were repeated 8 times. According to XRD and optical microscopy analyses the obtained substances were pure ghelenite and wollastonite (in the form of cyclowollastonite).

Methods

MA was performed in an AGO-2 planetary ball mill [8] at 40 g centrifugal factor. The initial sample mass was 10 g. The steel ball (5 mm in diameter) load to sample weight ratio was 20. Immediately before grinding, the air in the grinding vial was displaced by CO_2 from cylinder using higher density of carbon dioxide, and the vial was sealed hermetically. After 1, 2, 6, 10, and 20 min of MA about 1 g of sample was taken for analysis. After each sampling and every 2 min of MA the vial was repeatedly filled with CO_2 at $P=10^5$ Pa. According to chemical analysis of the silicate minerals samples after MA for 30 min in CO_2 atmosphere the milling yield was within 1.5–2.0 mass % Fe.

X-ray diffraction (XRD) data were measured using DRON-2 equipment (CuK_α radiation). IR spectra were recorded in potassium bromide pellets with a UR-20 spectrometer. The carbon dioxide amount absorbed by silicates during MA was determined volumetrically using an AN-7529 gas analyzer. A weighed portion of the sample was calcined at 1200°C and the released CO_2 was absorbed by strontium chloride solution resulting in its acidation. The obtained solution was neutralized by electric current and the amount of absorbed CO_2 was determined coulometrically. The minor amount of carbonate present in natural minerals due to presence of carbonate minerals as admixtures was subtracted from measured CO_2 content of the mineral samples after MA. The specific surface area was measured using FlowSorb II 2300 (Micromeritics) analyzer by the low temperature nitrogen adsorption method. Scanning electron microscopic (SEM) images were obtained on a Supra 50 VP, and TEM images were obtained on a JEOL JEM-2100F instruments. Before measurement the specimens were dispersed in ethanol by agitation for 10 min and then applied to collodion film and dried for 5–12 h.

Results and Discussion

XRD and IR measurements

Structural and chemical changes of the silicates in the course of MA in CO_2 atmosphere can be briefly reviewed for ghelenite as the example. XRD patterns and IR spectra of initial and MA-samples of ghelenite are shown in Figs. 1 and 2, respectively. As can be clearly seen, during the process of MA, substantial changes in the samples occur. Smoothing of IR bands visible in the 1100-400 cm^{-1} region can be explained by the silicate structure disordering and amorphization, which is supported by XRD measurements.

MA of ghelenite in CO_2 atmosphere, in agreement with earlier work [1-3], leads to the appearance of the double band near 1500 cm^{-1} corresponding to ν_3 antisymmetric stretching vibrations of CO_3^{2-} group (Fig. 2). The intensity of this band increases in the course of MA due to progressive sorption of carbon dioxide. Carbon dioxide content in MA-ghelenite after 30 min of mechanical treatment in planetary mill in CO_2 atmosphere reaches about 12 wt. % CO_2 that is equivalent to 27 wt. % $CaCO_3$ content in the mineral. Extensive CO_2 mechanosorption occurs alongside with silicate structure disordering and is not accompanied by formation of calcite or other carbonate minerals according to XRD data (Fig. 1).

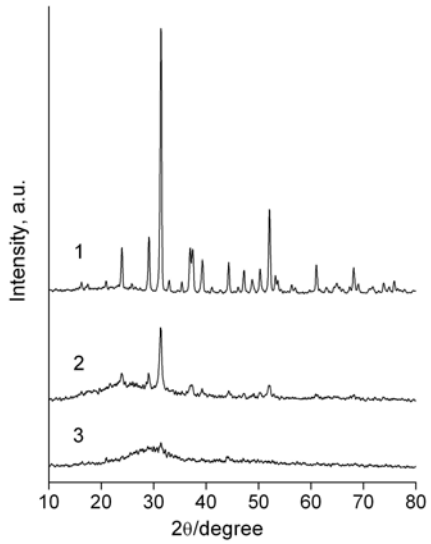

Figure 1. XRD patterns of ghelenite: 1 – initial sample; 2 and 3 – after 2 and 30 min of MA in CO_2 atmosphere, respectively

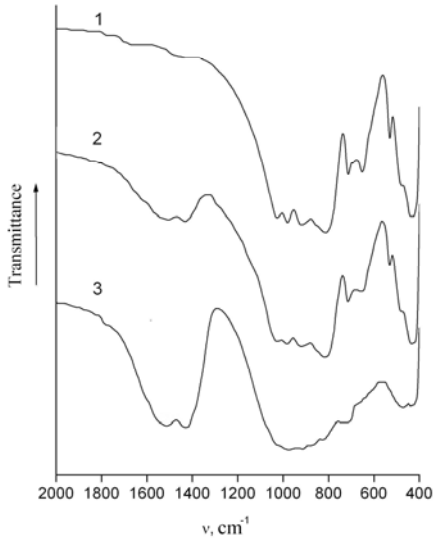

Figure 2. IR spectra of ghelenite. Designations are the same as in Fig. 1.

SEM and TEM Measurements

To verify the hypothesis of mechanically induced "dissolution" of carbon dioxide in the structurally disordered silicate with formation of homogeneous amorphous carbonate–silicate phase micro- and nanostructure of material resulting from mechanochemical interaction of diopside with CO_2 was investigated using SEM (Fig. 3) and TEM (Figs. 4-7).

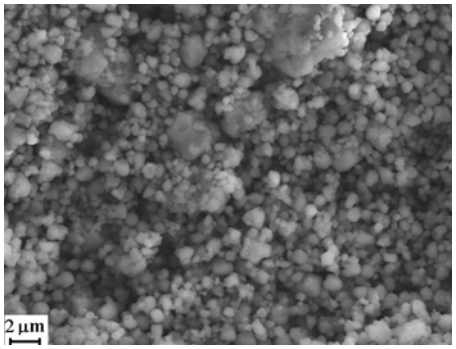

Figure 3. SEM image of MA-diopside

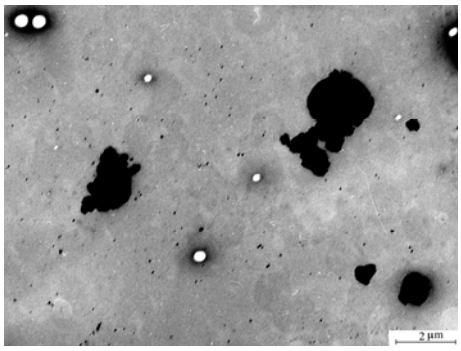

Fig. 4. TEM images of MA-diopside dispersed in ethanol and then applied to collodion film

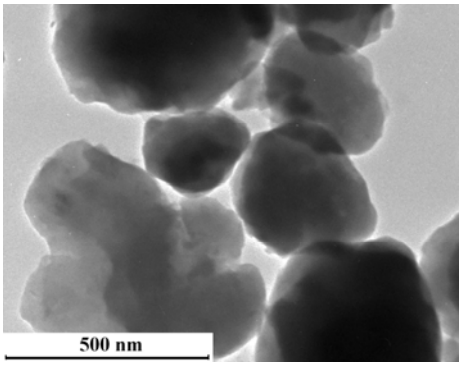

Fig. 5. TEM image of MA-diopside (500 nm length scale)

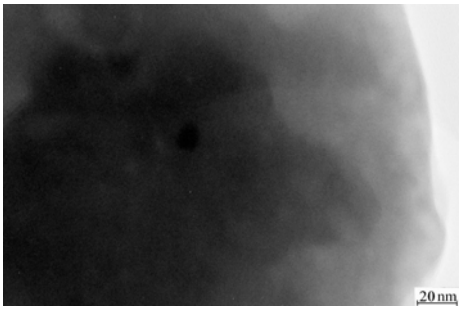

Fig. 6. TEM image of MA-diopside (20 nm length scale)

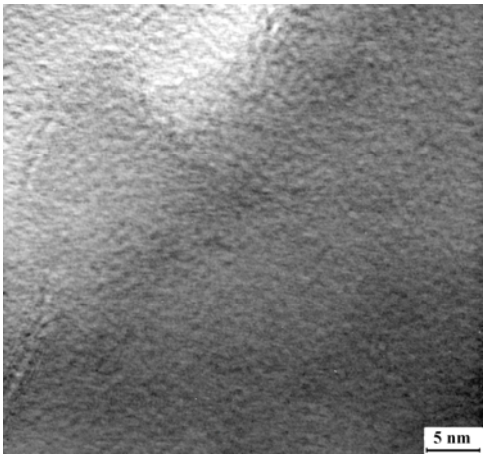

Figure 7. HRTEM image of MA-diopside (5 nm length scale)

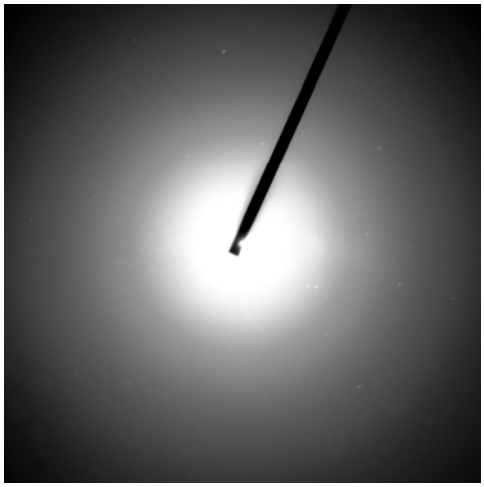

Figure 8. SAD pattern of the MA-diopside

The diopside sample was ground in a 75T-DRM vibratory mill for 65 h at $P(CO_2)=10^5$Pa. As a result, according to XRD data (not shown) the mineral was fully amorphized and the CO_2 content of the MA-diopside was 21.3 ± 0.8 wt %. SEM image of MA-diopside (Fig. 3) demonstrates that aggregation of particles took place after such prolonged grinding. The shape of particles and their aggregates were rather smooth. Dispersing the powder in ethanol insured partial disaggregation, as evidenced by TEM images, which showed ultrafine particles one to two orders of magnitude smaller (Fig. 4) than those observed by SEM (Fig. 3). More detailed information about the particle microstructure is provided by high- resolution TEM (HRTEM) image (Fig. 7). Note that no marked inhomogeneities were detected in the bulk of MA-diopside particles. The particles had smooth surfaces, with no sharp edges. The boundary between two overlapping particles was rather easy to discern (Fig. 5). Some of the MA-diopside particles contained inclusions about 10 nm in size - no more than one inclusion in a relatively large particle on the order of 0.5–1 μm in size. One inclusion is seen in Fig. 6. Presumably, the inclusions are either diopside nanocrystals or iron particles originating from the mill material. On the whole, the diopside activated in CO_2 has a homogeneous microstructure as evidenced by HRTEM images (Fig. 7) and selected area diffraction (SAD) patterns, characteristic of amorphous glass-like structure (Fig. 8).

The formation mechanism of this carbonate-silicate glass-like material appears to be related to arising and moving of structural defects and plastic behavior during MA [8-12]. Substantial enhance of transport processes due to plastic deformation in all probability plays here a special part - so called deformational mixing on molecular scale [11]. Besides, intercrystallite boundaries are channels of enhanced diffusion of adsorbed CO_2 molecules into the bulk of particles. Density of the intercrystallite boundaries network increases as the size of microcrystallites decreases in the course of MA. Decreasing of microcrystallites size to 10^{-9}-10^{-8} m increases the diffusion rate by several orders of magnitude [11].

Kinetics of CO_2 Mechanosorption by Silicates

Figure 9 shows carbonization degrees (mass % CO_2) of the studied silicates depending on MA time in CO_2 atmosphere. It follows from Fig. 9 that CO_2 content in wollastonite, ghelenite and okermanite samples is similar at the same MA time. Diopside and particularly labradorite exhibit lower mechanically induced carbon dioxide sorption ability. These data are in agreement with previously revealed tendency: the larger the calcium content in the mineral (see Table 1) the higher is its carbonization degree during grinding [1]. According to XRD data in the course of MA, crystal structure disordering of the samples increased. After 30 min of MA ghelenite sample (Fig. 1) and all other studied mineral samples (not shown) were almost completely amorphous.

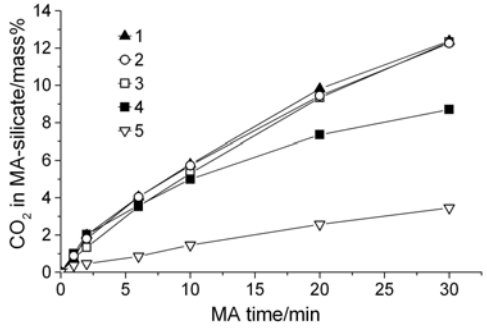

Figure 9. Carbonization degrees (mass % CO_2) of silicate minerals depending on MA time in CO_2 atmosphere: 1 – okermanite, 2 – wollastonite, 3 – ghelenite, 4 – diopside, 5 – labradorite

It follows from the slope of the curves (Fig. 9) that the intensity of carbonization process for all studied minerals gradually slows down with increase of MA time. It should be noted that the rigorous consideration of mechanosorption kinetics is a complicated problem due to variety of physical-chemical processes involved in mechanical action upon solid – gas system and their non-equilibrium nature [8-12]. Mechanism and kinetics of mechanically induced absorption of inert gases by metals and chemisorption of hydrogen onto quartz particles surface were

studied in [9] and [13], respectively. In the former case inert gases physically "dissolved" in the surface layer of metal under mechanical impact. In the latter one hydrogen molecules chemically reacted with free radical centers on the surface of quartz. As was mentioned above in the course of MA of silicates in CO_2 atmosphere carbon dioxide molecules both penetrated the structurally disordered mineral particles and chemically reacted with oxygen anions forming CO_3^{2-} groups [1-3]. Under these circumstances it is reasonable to determine the basic factors that influence mechanosorption and to apply a simplified model.

Two modes of gas sorption were revealed during study of quartz vibro-milling in H_2 atmosphere [13]. During initial stage of grinding mechanical energy was mainly spent for fresh surface formation. During this so called cleavage mode hydrogen molecules were chemisorbed on active centers of the newly formed surface. The rate of gas sorption in the cleavage mode was in direct proportion to the rate of active centers growth and consequently to the rate of surface area increase. As the total surface area S raised during grinding, portion of active centers arising due to friction of particles surface increased (so called friction mode). In the friction mode the rate of gas sorption depended on the surface area value instead of on the surface area time derivative as in the cleavage mode. The total rate of gas sorption W can be expressed as [13]:

$$W = W_{cl} + W_{fr} = a(dS / d\tau) + f_{fr}(S) \quad (1)$$

where W_{cl} and W_{fr} are the rates of gas sorption induced by cleavage and friction, respectively; a – coefficient that is proportional to the active centers concentration on the fresh surface. Contribution of friction to the total rate $W_{fr} = f_{fr}(S)$ depends not only on the surface area but also on type of grinding, nature of gas and solid, and other factors. The analytical form of $f_{fr}(S)$ is unknown. Using this general scheme we can consider carbon dioxide mechanosorption by the silicate minerals.

A typical change of mineral specific surface area during MA as a function of MA time and mechanical energy dose is shown in Fig. 10 by the example of ghelenite.

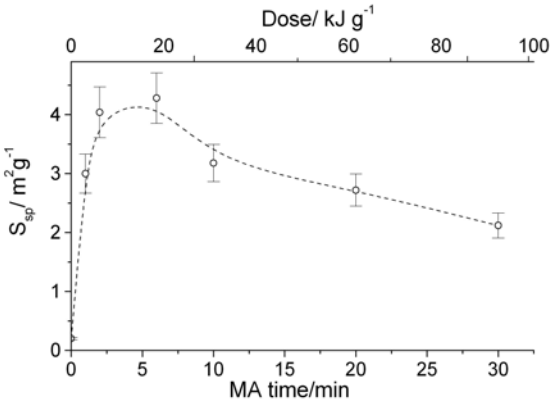

Figure 10. Specific surface area of ghelenite depending on MA time in CO_2 atmosphere

The curve in Fig. 10 can be divided into two parts. During the first 1-2 min of MA the specific surface area S_{sp} rapidly increased. Then S_{sp} gradually decreased due to aggregation processes and turned to quasi-steady state. It is reasonable to assume that during the first 2 minutes of MA mechanosorption occurred mainly in the cleavage mode and partially in the friction one. After maximum (more than 2 min of MA) CO_2 sorption was virtually totally controlled by friction. During the first 1-2 min of MA in CO_2 atmosphere silicate particles with carbonized thin surface layer were formed. At this stage (the cleavage mode) the intensity of CO_2 sorption was the highest one (Fig. 9). Then dispersion, i.e. reducing of particles size and growth of surface area, stopped due to the size factor and aggregation processes [8,9] (Fig. 10). Sorption of carbon dioxide by the silicates became slower at this stage because CO_2 molecules diffused inside the structurally disordered particles through the outer carbonized layer. It should be noted, that despite the notable decrease of surface area after 2 min of MA (Fig. 10) the rate of CO_2 sorption slowed down to only a small extent (Fig. 9). This is evidence that after 2 min of MA sorption mainly occurred in the friction mode. In IR spectra of MA-silicates in 2370-2350 cm^{-1} region (not shown) there were no bands corresponding to physically adsorbed CO_2 or to carbon dioxide dissolved in molecular form [1-3]. Thus under intensive mechanical treatment resulting in accumulation of defects, deformation and break of bonds not only on the surface but also in the bulk of silicate particles, the rate of chemical interaction

$$CO_2 + O^{2-} = CO_3^{2-}$$

was high and the mechanosorption process as a whole was diffusion controlled.

Consider CO_2 mechanosorption by a silicate at MA time more than 2 min that is in the friction mode. Equation (1) can be rewritten in the form

$$W = W_{fr} = f_{fr}(S) \quad (2)$$

Mechanosorption rate is determined as $W = dM/d\tau$, where M – total mass of CO_2 absorbed by a silicate, S – total surface area of a solid. Applying Fick's laws of diffusion in semi-infinite solid approximation [14] one can derive

$$W = f_{fr}^{(s)} = dM / d\tau = K_{ms}(S^2 / M) \quad (3)$$

where K_{ms} – mechanosorption coefficient ($g^2m^{-4}min^{-1}$). Actually K_{ms} is a semi-empirical parameter that characterizes mechanosorption ability of silicate with respect to carbon dioxide. Equation (3) can be transformed taking into account changing of S in the course of MA. M and S can be written in the form

$$M = 0.01C \cdot q /(1 - 0.01C) \quad (4)$$

$$S = S_{sp} \cdot q /(1 - 0.01C) \quad (5)$$

where q – initial mass of mineral (g), C – carbonization degree expressed as mass % CO_2 in MA-mineral, S_{sp} - specific surface area of MA-mineral (m^2g^{-1}). One should bear in mind that both

C and S_{sp} depend on MA time. After substitution of (4) and (5) in (3) and some rearrangement one can derive

$$-d\ln(1-0.01C) = 10^2 K_{ms}\frac{S_{sp}^2}{C}d\tau \qquad (6)$$

Integration of Eq. (6) from τ = 2 min to τ = t min (the friction mode) leads to

$$F(t) - F(2) = 10^2 K_{ms}\int_2^t \left(\frac{S_{sp}^2}{C}\right)d\tau = 10^2 K_{ms}\Theta(t) \qquad (7)$$

where

$$F(t) = \ln(1-0.01C(t)) \qquad (8)$$

$$\Theta(t) = \int_2^t \left(\frac{S_{sp}^2}{C}\right)d\tau \qquad (9)$$

For calculation of Θ(t) experimental values of S_{sp}^2/C were fitted by least-squares method using the following expression

$$S_{sp}^2 / C = b_0 + b_1\exp(-b_2\tau) + b_3\exp(-b_4\tau) \qquad (10)$$

A typical agreement between the experimental values of S_{sp}^2/C and the calculated ones using Eq. (10) is shown for ghelenite as the example in Fig. 11.

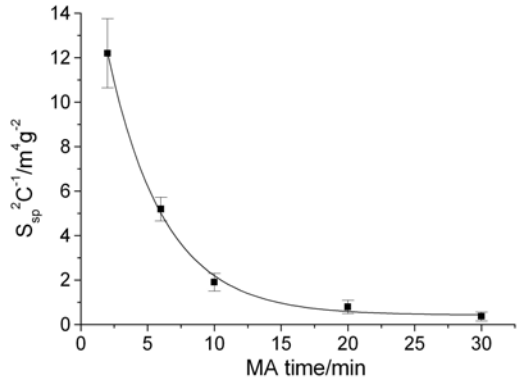

Figure 11. Experimental values of S_{sp}^2/C for ghelenite (squares) and approximation curve according to Eq. (10) (solid line)

Using Eq. (10) Θ(t) can be calculated in the form

$$\Theta(t) = b_0(t-2) - \frac{b_1}{b_2}\left[\exp(-b_2 t) - \exp(-2b_2)\right] - \frac{b_3}{b_4}\left[\exp(-b_4 t) - \exp(-2b_4)\right] \qquad (11)$$

For ghelenite [F(t)-F(2)] values obtained by substitution of experimental C(t) values to Eq. (8) plotted against Θ(t) calculated using Eq. (11) are shown in Fig. 12.

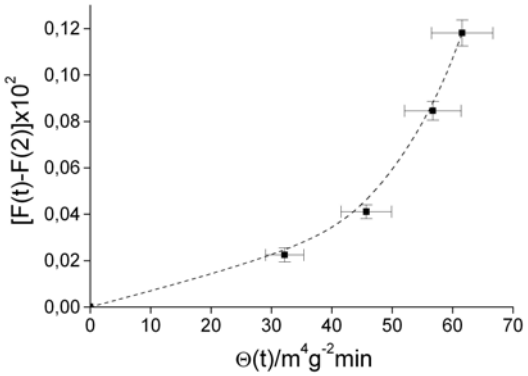

Figure 12. [F(t)-F(2)] values depending on Θ(t) for MA of ghelenite (see text for details)

Squares in Fig. 12 from left to right correspond to 2 (point of origin), 6, 10, 20, and 30 min of MA, respectively. Provided that K_{ms} in Eq. (7) is constant, points in Fig. 12 would display linear dependence with slope being equal to 10^2K_{ms}. However from Fig. 12 it follows that mechanosorption coefficient grew with increase of MA time. It can be explained by the following reason. In the course of MA due to accumulation of defects the silicate mineral structure disordering substantially increased (Fig. 1) thereby facilitating diffusion process.

In order to take into account the growth of mechanosorption coefficient with increase of MA time K_{ms} can be inserted into Eq. (7) in the form

$$K_{ms}(\tau) = k_0 + k\tau \qquad (12)$$

where k_0 and k are empirical parameters, τ is MA time, min. Substitution of Eq. (12) in (6) and integration yield

$$F(t) - F(2) = 10^2(k_0\Theta(t) + k\Psi(t)) \qquad (13)$$

Where

$$\Psi(t) = \int_2^t \left(\frac{S_{sp}^2}{C}\right)\tau d\tau \qquad (14)$$

Ψ(t) can be easily calculated after substitution of Eq. (10) in (14). For evaluating of k_0 and k it is convenient to introduce Φ(t) and Ω(t):

$$\Phi(t) = 10^{-2}\frac{F(t) - F(2)}{\Theta(t)} \qquad (15)$$

$$\Omega(t) = \frac{\Psi(t)}{\Theta(t)} \qquad (16)$$

Φ(t) values against Ω(t) are plotted in Fig. 13. Straight line in Fig. 13 corresponds to linear least-square fit of the points. The slope and intercept of the line are equal to k_0 and k in Eq. (13), respectively.

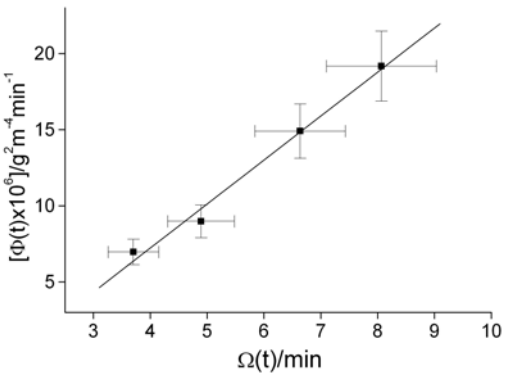

Figure 13. Φ(t) values depending on Ω(t) for MA of ghelenite. From left to right squares corresponded to 6, 10, 20, and 30 min of MA, respectively (see text for details)

For ghelenite mechanosorption coefficient was expressed in the form

$$K_{ms}(\tau) = -(4.3 \pm 0.4)10^{-6} + (2.9 \pm 0.3)10^{-6}\tau \quad (13)$$

($g^2m^{-4}min^{-1}$)

Note that extrapolation of Eq. (17) beyond the range of points plotted in Fig. 13, corresponding to time interval from 6 to 30 min of MA may lead to unreasonable results. Calculation of carbonization degrees C in the sampling points (6, 10, 20, and 30 min of MA) from obtained k_0 and k values (Table 2) using Eqs. (11)-(14) showed that standard deviation between the experimental (Fig. 9) and the calculated values for all studied minerals was 0.28 mass % CO_2. So in spite of the simplified approach, the suggested semi-empirical equations reasonably good described CO_2 mechanosorption kinetics. One should bear in mind that generally K_{MS} depends on type of mill, mill load, and MA time. The comparison of K_{MS} values determined for different minerals is valid if only MA is carried out at the same conditions.

Correlations with Dissolution of CO_2 in Melts

As was mentioned above mechanically induced absorption of carbon dioxide by silicate minerals in a certain way resembles dissolution of CO_2 in silicate melts of similar composition at magma state conditions. It is interesting to compare the carbonization degrees of minerals after MA and solubility of CO_2 in silicate melts having the same composition. In geochemical literature interaction of CO_2 and other gases (or fluids) with silicate melts is a subject of narrow investigation because even small amount of the dissolved volatile may notably affect physical and chemical properties of magma and as a result its evolution path (see, for example [15,16]). At the same time experimental solubility data for various melt compositions have been determined at different pressures and temperatures and their direct comparison is rather difficult.

Table 2. Calculated b_i coefficients (i=0,1..4) in eqs. (10),(11) and k_0 and k coefficients in Eq. (12)

coefficient	labradorite	diopside	okermanite	ghelenite	wollastonite
b_0, m^4g^{-2}	11.687	0.9390	-24.281	0.42229	3.3631
b_1, m^4g^{-2}	174.703	27.8744	20.4583	11.890	23.2045
b_2, min^{-1}	0.12575	0.71481	0.26967	0.23697	0.25916
b_3, m^4g^{-2}	- 34.199	13.0665	25.2847	7.0824	-4.3228
$b_4 \cdot 10^2$, min^{-1}	3.6342	11.602	0.0323	23.709	1.46
$k_0 \cdot 10^6$, $g^2m^{-4}min^{-1}$	-0.091 ±0.009	2.5 ±0.3	-0.42 ±0.4	-4.3 ±0.4	-9.1 ±0.9
$k \cdot 10^6$, $g^2m^{-4}min^{-2}$	0.052 ±0.005	0.34 ±0.03	1.9 ±0.2	2.9 ±0.3	4.4 ±0.4

In this paper, semi-empirical thermodynamic model advanced by Papale [17] has been used to calculate CO_2 solubility at fixed T and P in melts having the same compositions as the studied minerals. The model [17] was formulated assuming mechanical, thermal and chemical equilibrium between liquid magma and gas (fluid) phase. CO_2 fugacity in the fluid phase was calculated using Kerrick and Jacobs modified Redlich-Kwong equation of state for gaseous carbon dioxide [18]. Activity coefficients of CO_2 dissolved in liquid phase were determined in [17] on basis of strictly regular solution theory for volatile-free magma [19] and assuming P-dependent binary interaction coefficients for carbon dioxide (non-isometric mixing). It should be noted that CO_2 is present in MA-silicates only as carbonate group [1-4], while dissolution of carbon dioxide in magmatic melts occurs in two forms: CO_3^{2-} ion (the major form for the silicate compositions studied here) and molecular CO_2 [15]. Model [17] enables to calculate the total CO_2 solubility in melts.

For calculation of carbon dioxide solubility in silicate melts T=1900K and P=1.5 GPa were chosen because at this temperature and pressure all silicates considered here are liquid. In addition, CO_2 solubility in the melt at chosen T and P is comparable with mechanically induced carbonization degree of the silicate having the same composition. Calculated CO_2 solubility in melts and corresponding CO_2 content in the silicates of the same composition after 30 min MA in carbon dioxide atmosphere are shown in Fig. 14. It is seen that there is surprising very good correlation for labradorite, diopside and okermanite (dashed line in Fig. 6) but wollastonite and ghelenite fall out this trend. Certainly the number of points is too small for reliable correlation analysis. However one should take into account that errors of calculated CO_2 solubility in case of wollastonite and ghelenite melts are larger because their composition to a certain extent fall out of the model calibration range due to high calcium content [17] (see Table 1).

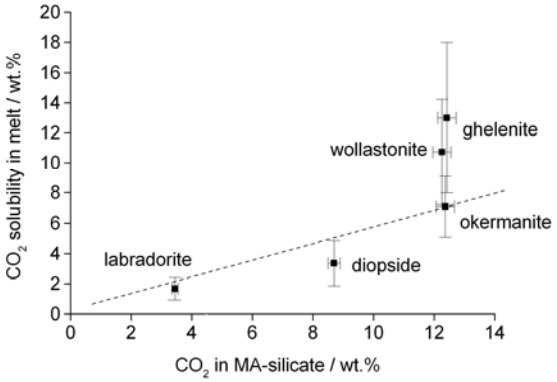

Figure 14. Calculated CO_2 solubility in melts at T=1900K and P=1.5GPa plotted against CO_2 content in silicates after 30 min of MA in carbon dioxide atmosphere. For each point volatile-free melt composition is identical to the corresponding mineral composition

In addition to equilibrium solubility data it is interesting to compare CO_2 diffusion in silicate melts with carbon dioxide mechanosorption kinetics. Published experimental data indicate that at constant temperature in the range of carbon dioxide content less than 1 wt. % CO_2 diffusion coefficient D keeps nearly constant with wide changing of melt composition [20-22]. Unfortunately no diffusion data are available for higher CO_2 concentration in melts. However concentration dependence of D can be evaluated using standard relation [14]

$$D = D_0 \frac{\partial \ln a}{d \ln x} = D_0 \frac{\partial \ln(\gamma x)}{\partial \ln x} \qquad (18)$$

Here a, γ, and x – activity, activity coefficient, and molar fraction of CO_2 in melt, respectively; D_0 – diffusion coefficient assuming γ=1. Derivation in Equation (18) can be easily implemented within thermodynamic model used above for solubility calculation [17]. It is reasonable to assume that D_0 corresponds to the carbon dioxide diffusion coefficient experimentally determined for melts having small CO_2 concentrations. Note that D_0 is not sensitive to melt composition, so it can de used for all silicates at given T,P-conditions. One should mention as well that CO_2 diffusion coefficient is strongly temperature dependent following Arrhenius equation and to much lesser extent is pressure dependent [22]. From carbon dioxide diffusion data presented in [22] it is possible to accept $D_0 \approx 1 \cdot 10^{-9}$ $m^2 \cdot s^{-1}$ at T = 1900 K and P = 1.5 GPa. Figure 15 shows calculated D values (T = 1900 K, P = 1.5 GPa) plotted against K_{ms}. For each mineral mechanosorption coefficients were evaluated according to Equation (12) using k and k_0 derived from carbonization degree data as described above. For comparison purposes D and K_{ms} were calculated for each mineral at the same CO_2 concentration both in melt and in MA-silicate being equal to half of the silicate carbonization degree in the end of MA experiment. This CO_2 content approximately corresponds to 10 min of MA for each mineral (Fig. 9). As in case of solubility and carbonization degree (Fig. 14) here labradorite, diopside and okermanite points fit linear interpolation very well. Lower precision wollastonite and ghelenite data points fall out (Fig. 15). Solid line in Fig. 15 corresponds to linear fit of all plotted data.

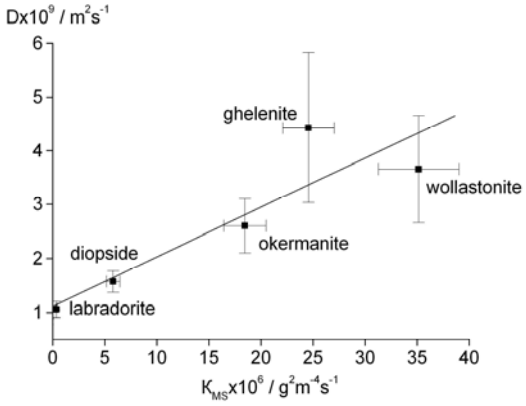

Figure15. Calculated CO_2 diffusion coefficients (D) for melts at T=1900K and P=1.5GPa plotted against CO_2 mechanosorption coefficients (K_{ms}). D and K_{ms} values were determined at the same carbon dioxide content in melt and in the corresponding MA-silicate (see text for details)

<u>CO_2 Mechanosorption by Ferrous-magnesium Slag: Application for Alkali-Activated Slag Binding Materials</u>

In this section the research object was granulated ferrous-magnesium slag from Pechenganickel smelter plant, Murmansk Region, Russia. Chemical composition of the slag (wt. %): SiO_2 - 40.88, Al_2O_3 - 6.90, FeO - 35.40, MgO - 10.71, CaO - 2.65, (Na_2O+K_2O) – 2.1, S - 0.71. Mineral composition of the slag (mass. %): ferrous-magnesium silicate glass – 95-98, olivine – 2-5, Cu-Ni sulfides – 1-3. It is known that ferrous-magnesium slag reacts with sodium hydroxide solution or liquid glass producing hardened material. The properties of the alkali-activated slag (AAS) binding material depend on interaction between the ground slag surface and alkali containing component. The reactivity of powder surface may change during grinding, particularly due to mechanically induced sorption of gases. Ferrous-magnesium slag is a silicate material containing magnesium, calcium and alkali metal oxides. So, one may expect carbon dioxide sorption by the slag during mechanical treatment in mill in CO_2 atmosphere. We have performed MA of the slag in air and in CO_2 atmosphere in order to investigate the role of carbon dioxide mechanosorption on its binding properties.

Grinding of the slag was performed in an AGO-2 planetary ball mill at 40 g centrifugal factor. The slag mass was 20 g. The steel ball (8 mm in diameter) load to slag weight ratio was 10. The maximum grinding time was 330 sec. Carbon dioxide content in the slag samples after 330 sec of grinding in air and in CO_2 at $P(CO_2)=10^5$ Pa was 0.20±0.03 and 0.50±0.05 wt.% CO_2, respectively. Ground slag was mixed with liquid glass to obtain normal density paste using following conditions: liquid glass module – 1.5, Na_2O content – 5% with respect to weight of the ground slag, water to slag weight ratio – 0.23. Samples 1.41×1.41×1.41 cm in size were molded from the paste. Hardening of the samples was carried out in humid atmosphere at 20-22°C.

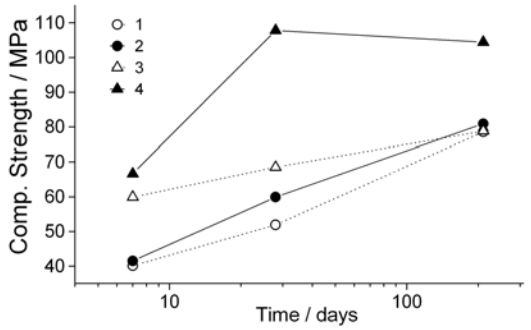

Figure16. Compressive strength of AAS samples. S_{sp} of ground slag: 1 – 410, 2 - 450, 3 – 750, 4 – 730 m^2kg^{-1}, respectively. Grinding atmosphere: open symbols and dashed lines – air; solid symbols and solid lines – CO_2

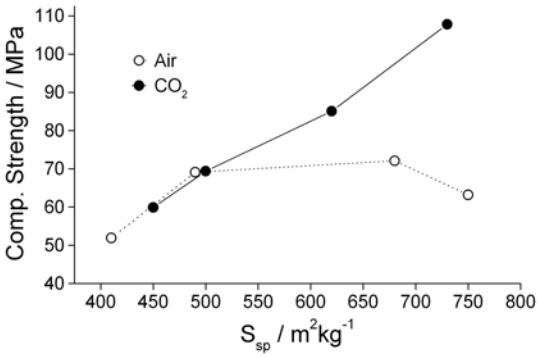

Figure17. Compressive strength of AAS samples aged for 28 days as a function of ground slag S_{sp} and grinding atmosphere

Figure 16 shows compressive strength of AAS samples for ground slag specific surface area (S_{sp}) ca. 400 and 700 m^2kg^{-1} as a function of ageing time. It is seen that preliminary grinding in CO_2 promotes hydration processes and leads to higher compressive strength in comparison to grinding in air. Compressive strength of AAS samples aged for 28 days as a function of ground slag S_{sp} are shown in Fig. 17. From the obtained data it follows that positive effect of grinding in carbon dioxide increases with growing of ground slag specific surface area. It can be explained by lager slag carbonization degree at higher S_{sp}. It should be noted that compressive strength of AAS samples obtained using grinding in CO_2 reaches 100-110 MPa (Figs. 16 and 17).

Conclusions

It has been shown that in accordance with the results obtained earlier, mechanical activation of labradorite, diopside, okermanite, ghelenite, and wollastonite in CO_2 atmosphere in a laboratory ball planetary mill results in extensive sorption of carbon dioxide molecules by the minerals and their "dissolution" in the structurally disordered silicate matrix in the form of distorted carbonate groups.

The suggested equations can be used for simplified kinetic analysis of mechanically induced CO_2 sorption by silicates. Mechanosorption coefficient K_{ms} can serve as semi-empirical parameter to characterize ability of silicate to absorb carbon dioxide in the course of MA. In this study, high energy input AGO-2 planetary mill has been used for MA resulting in bulk sorption of CO_2 by the silicates. In order to determine the optimal energy input and type of mechanical treatment for effective carbon dioxide sorption further investigation is needed. Water present in the mill certainly plays an important role in the CO_2 mechanosorption by silicates. For elucidating the role of water, MA experiments with various amounts of H_2O added to mineral should be carried out.

The observed correlations support the hypothesis of similarity between carbon dioxide mechanosorption and CO_2 dissolution in melts. It should be emphasized that at first glance the two very dissimilar processes are compared here. Carbon dioxide dissolution in melt occurs at high temperatures and pressures. In addition, CO_2 solubility characterizes true thermodynamic equilibrium between the gas (fluid) and liquid. Silicates consume CO_2 during mechanical treatment as a result of essentially non-equilibrium process occurring at ambient conditions. Nevertheless the observed correlations apparently reflect the resemblance in nature of these processes.

It has been revealed that preliminary grinding of ferrous-magnesium slag in CO_2 promotes hydration processes and leads to higher compressive strength of alkali-activated slag binding materials in comparison to grinding in air. The reason for this is probably an increase in slag reactivity due to mechanosorption of carbon dioxide by the outer layer of the slag particles.

Acknowledgements

The financial support of Russian Foundation for Basic Research (grant № 06-03-32198) is gratefully acknowledged. Author is grateful to Dr. E.V. Kalinkina, Dr. B.I. Gurevich, Dr. V.V. Tyukavkina and Mr. O.A. Zalkind for their help in carrying out the experiments and fruitful discussions.

References

1. E.V. Kalinkina, A.M. Kalinkin, W. Forsling, and V.N. Makarov, *Int. J. Miner. Process.,* 61 (2001) 273.
2. A.M. Kalinkin, A.A. Politov, V.V. Boldyrev, E.V. Kalinkina, V.N. Makarov, and V.T. Kalinnikov, *J. Mater. Synt. Proc*., 10 (2002) 61.
3. A.M. Kalinkin, E.V. Kalinkina, A.A. Politov, V.N. Makarov, and V.V. Boldyrev, *J. Mater. Sci.,* 39 (2004) 5393.
4. A.M. Kalinkin, E.V. Kalinkina, O.A. Zalkind and T.I. Makarova, *Inorg. Mater*., 41 (2005) 1073.
5. A.M. Kalinkin, E.V. Kalinkina, O.A. Zalkind, and T.I. Makarova, *Colloid Zh*., 70 (2008) 33.
6. A.M. Kalinkin, E.V. Kalinkina, O.A. Zalkind, and T.I. Makarova, *Colloid Zh*., 70 (2008) 42.

7. W.A. Deer, R.A. Howie, and J. Zussman, *An Introduction to the Rock-Forming Minerals*, Longman, London (1992).
8. E. G. Avvakumov, *Mechanical Methods of Activation of Chemical Processes*, Nauka, Novosibirsk (1986). (in Russian)
9. G. Heinicke, *Tribochemistry*, Carl Hanser Verlag, München, Wien (1984).
10. V.V. Boldyrev, *Russ. Chem. Rev*., 75 (2006) 177.
11. P.Yu. Butyagin, *Russ. Chem. Rev*., 63 (1994) 965.
12. G.S. Khodakov, *Colloid Zh*., 56 (1994) 113.
13. A.N. Streletskiy and P.Yu. Butyagin, *Kinetika i Kataliz*, 21 (1980) 770. (in Russian)
14. A.A. Zhukhovitskiy and L.A. Schwarzman, *Physical Chemistry*, Izd. Lit. Tsvet. Cher. Met., Moscow (1963), p. 463. (in Russian)
15. J.G. Blank and R.A. Brooker, in *Reviews in Mineralogy. V. 30. Volatiles in Magmas,* (eds.) M.R. Carroll and J.R. Holloway, Mineralogical Society of America, Washington DC (1994), p. 158.
16. R. Botcharnikov, M. Freise, F. Holtz, and H. Behrens, *Ann. Geophys*., 48 (2005) 633.
17. P. Papale, *Am. Mineral*., 84 (1999) 477.
18. D.M. Kerrick, and G.K. Jacobs, *Am. J. Sci*., 281 (1981) 735.
19. M.S. Ghiorso, I.S.E. Carmichael, M.L. Rivers, and R.O. Sack, *Contrib. Mineral. Petrol.*, 84 (1983) 107.
20. E.B. Watson, M.A. Sneeringer, and A. Ross., *Earth Planet. Sci. Lett*. 61 (1982) 346.
21. M. Nowak, D. Schreen, and K. Spickenbom, *Geochim. Cosmochim. Acta*, 68 (2004) 5127.
22. D.R. Baker, C. Freda, R.A. Brooker, and P. Scarlato, *Ann. Geophys*., 48 (2005) 699.